
Detection of transient time lapse seismic signatures associated with CO₂ injection

Kris Innanen, Don Lawton, Kevin Hall, Kevin Bertram and Malcolm Bertram

ABSTRACT

In 2018 CREWES researchers reported on a collaboration with JOGMEC in interpreting an unusual time-lapse data set, in which cross-well waveforms transiting a plume of injected microbubble water were seen to undergo several difficult-to-explain alterations. In addition to attempting to explain these phenomena, we also undertook to seek similar variations in seismic waveforms propagated through the plume of CO₂ being injected into the 300m formation at the CaMI-FRS in Newell County AB. In 2019 we expanded on that experiment, carrying out a 160hr set of repeated seismic shots taken during pressuring up, injection, and then pressuring down. We observe remarkable repeatability in the waveforms generated with the Vibroseis source, which was fixed with pad down throughout, and sensed with permanent 3C geophones cemented behind casing in the CaMI geophysics well. On this backdrop, with variability due to any source other than the pressure and fluid changes caused by the injection minimized, we examined the data. We identified several spectral variations which appear and then vanish over the course of the experiment. Because at each “cluster” of shots we repeated the sweep anywhere from 5 to 29 times, we can attach error bars to the spectral measurements; the changes we identified generally exceed these error bars significantly, often by roughly an order of magnitude. The changes are consistent those leading to our 2018 *elastic bracing* explanation, in that lower frequencies tend to decay (and then relax) and higher frequencies tend to boost (and then relax). They are however more subtle, though this may be because on the scale determined by the dominant wavelengths and injection depths of this experiment, the CO₂ plume is much smaller than was the microbubble injection zone.

INTRODUCTION

Last year we published a report and an SEG abstract in which two incidences of changes in the seismic waveform after fluid injection were noted (Innanen et al., 2019). We proposed a macroscopic description of the phenomena, pointing out that many – perhaps all – of the waveform changes could be accounted for by exchanging the standard elastic wave theory with a Klein-Gordon type equation, implying that some type of elastic “bracing” was operating (Morse and Feshbach, 1953). This turned out to be quite a timely observation, occurring at almost the same time a report appeared in *The Leading Edge* of transient seismic signatures occurring in association with reservoir stimulation (Byerley et al., 2018), which appeared and then dissipated long before a conventional time-lapse experiment would likely have been acquired. This year, we took these results as motivation to carry out a time-lapse VSP seismic experiment over the course of a short CO₂ injection program. Our aim was to inject CO₂ into a shallow formation in as well-characterized a manner as possible, and repeat a seismic shot whose raypaths crossed the expected fluid and pressure plumes at regular intervals, seeking evidence of transient waveform changes. In contrast to standard time lapse surveys (e.g., Landrø, 2001; Lumley, 2001), we specifically seek perturbations which appear in the short term, and are either sustained or vanish.

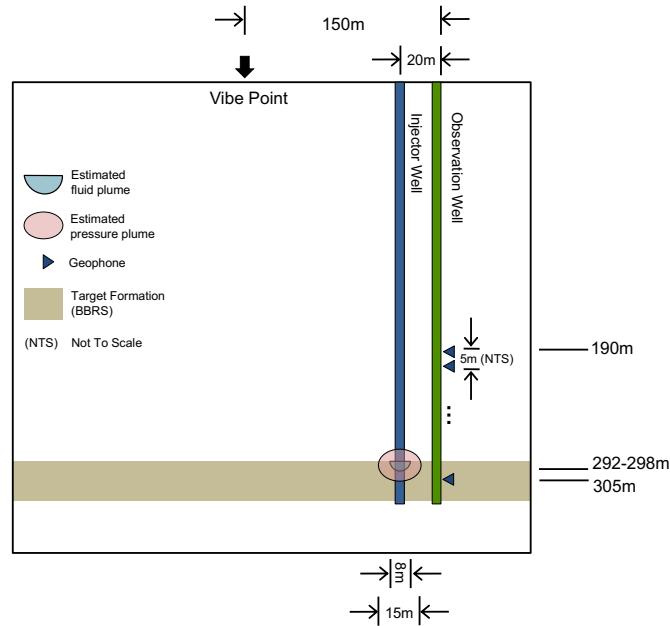


FIG. 1. Geometry and scale of seismic source, injection and observation wells, expected CO₂ / pressure plumes, and seismic sensors.

The Containment and Monitoring Institute Field Research Station (CaMI-FRS) in Newell County Alberta, which is part of Carbon Management Canada, offered a convenient opportunity to carry out such an experiment, as CO₂ injection was scheduled to come online in 2019. Prior to the main injection program, and subsequently during downtimes in injection pressure, have been prime opportunities to bring pressure up, inject for a period of time, and then relax the pressure, all the while shooting into the permanent array of 3C geophones cemented behind casing in the CaMI geophysics observation well.

EXPERIMENTAL CONFIGURATION AND INJECTION TIMELINE

The experiment involved placing the University of Calgary Envirovibe Source at a fixed point, lowering the pad, and leaving it there with pad down over the course of 7 days, repeating sweeps throughout. Just after the baseline data were acquired, the injection well was pressured up, commencing injection. After several hours, the pump was pressured down and the system was permitted to lapse back to a quiet state. By the end of the 160hr program the pressure had returned to its pre-injection level.

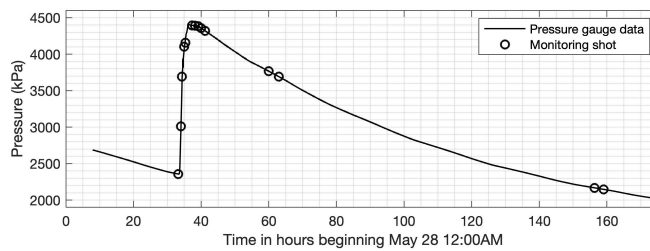


FIG. 2. Pressure data at injection point (black curve) versus time in hours from 00:00 May 28 2019. Circles are the times at which each of the 14 monitoring shot clusters occurred.

Geometry and scale

The source was positioned 150m from the observation well such that the injection well lay between the two. The CO₂ entered the Basal Belly River Sandstone (BBRS) formation, forming pressure and fluid plumes between depths of 290-305m. The plumes are estimated to be roughly 15m and 8m in diameter respectively, based on the injection/pressure timeline involved. The 24 3C geophones begin at 190m and end just below the plume locations at 305m. The basic geometry and scale of the experiment is summarized in Figure 1.

Auxiliary injection data

Our interest is to correlate changes in the seismic waveforms transiting the injection zone with quantities descriptive of the fluid entering the zone under pressure, and, should such changes exist, their evolution as the system lapses back to its original (or new equilibrium) state. Our main indicator of the state of the injection zone is the pressure data sensed near the point of injection. These data are plotted in Figure 2 (black curve), overlain with the points during the experiment at which monitoring data were acquired.

DATASET OVERVIEW

A total of 203 shots were taken over the 160hr experiment; these occurred in 14 clusters, with between 5 and 29 shots taken in rapid succession within each cluster (see Table 1 for details). The source was the 8000kg University of Calgary Envirovibe, which was programmed with a linear 10-150Hz sweep. The sensors were 3C geode geophones cemented behind casing. A visual inspection of the data was carried out after the experiment and 6 representative levels were selected based on overall data quality. Of these, the deepest was level 17 (approximately 275m); the shallowest was level 8 (230m).

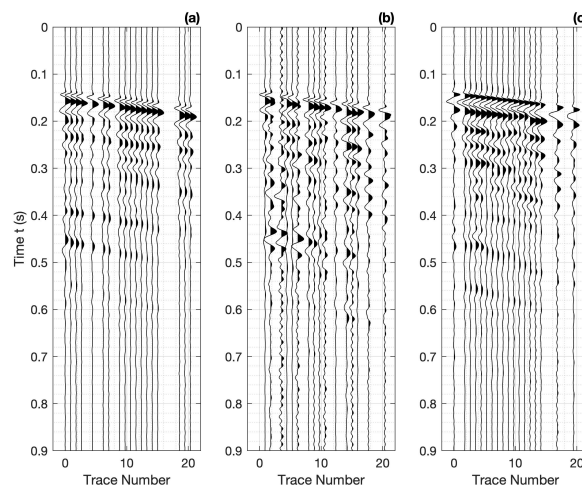


FIG. 3. Monitoring shot cluster 6, 1:30PM May 29 2019, shot 2 of 29. (a) Vertical component; (b) first horizontal component; (c) second horizontal component.

An example set of shot records is illustrated in Figure 3. In (a) the vertical component is illustrated, with the two horizontal components illustrated in (b)-(c). Traces have been killed at bad geophone levels. The first arrivals on all components are identifiable as down-

going P-waves with an apparent velocity of roughly 2800m/s; between 0.4-0.5s downgoing S-wave energy is also visible with apparent velocity near 1500m/s. In some of the shots electrical noise (from a battery charger) contaminated the data at 60Hz. We have in light of this restricted our analysis to frequencies $< 60\text{Hz}$.

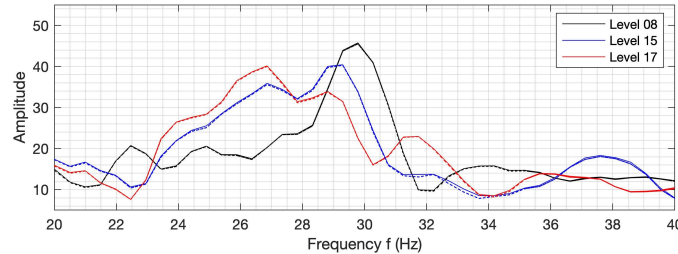


FIG. 4. Variation of the peak frequency with depth at a particular monitoring shot (N.B., not time-lapse variations). There is some evidence of attenuation in the data, with the peak frequency dropping by roughly 2Hz over the 50m interval between levels 8 and 17.

The time-lapse variability we will discuss appears to be most easily visible in the frequency domain. Let us begin by illustrating the significant changes in spectra from geophone level to geophone level at a single shot. In Figure 4 we compare spectra associated with the vertical component signal at three levels produced during a single monitoring shot cluster. A significant spectral shift of roughly 2Hz is clearly evident over the roughly 50m interval between the top and bottom geophone levels, suggestive of attenuation. Our focus will now shift to fixed geophone levels, and variations as a function of monitoring shot number.

Monitor #	Date	Time	# shots
1	May 29	9:20AM	5
2	May 29	10:00AM	6
3	May 29	10:30AM	5
4	May 29	11:00AM	5
5	May 29	11:30AM	9
6	May 29	1:30PM	26
7	May 29	2:40PM	11
8	May 29	3:15PM	14
9	May 29	4:00PM	20
10	May 29	5:15PM	15
11	May 30	12:00PM	29
12	May 30	3:00PM	29
13	June 03	12:30PM	15
14	June 03	3:00PM	14

Table 1. Monitoring shot cluster, dates/times, and number of sweeps per cluster.

Processing

The philosophy we took was to do a bare minimum of processing, because we had little idea going in of if variability would be identified, and if it was in what form it would appear. With that in mind, we made the following two changes to the raw data:

1. We corrected several polarity reversals;
2. We normalized each trace to its maximum value prior to Fourier transform.

This took the place of any candidate normalization of the spectra (e.g., transformation to db down). This would allow us to avoid choosing a particular frequency at which to enforce agreement between spectra, and instead tend to balance the overall area under one spectrum relative to another.

REPEATABILITY

For any candidate time-lapse variation associated with injection pressure and/or fluid to be convincingly identified, it must exceed the background variability, or scatter, of repeated seismic measurements. To permit the background variability from shot to shot to be characterized each monitoring cluster contains multiple repeated sweeps, anywhere between 5 and 29. The actual number within each cluster was determined in part by practical considerations; generally smaller numbers occur in situations where communication between the shot controlling computer and the source was temporarily interrupted.

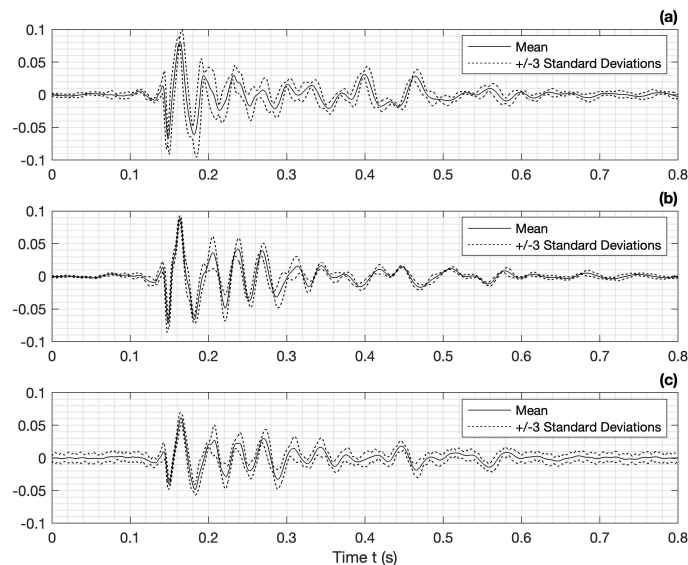


FIG. 5. Mean (solid) plus and minus three standard deviations (dashed) traces from the 9:20AM 6-shot monitoring survey, geophone level 6 of 24. (a) Vertical component; (b) first horizontal component; (c) second horizontal component.

The repeatability is summarized in four figures. In each figure a single representative geophone level has been selected, and the responses of all three components at that level are plotted. The first two figures illustrate the repeatability within the first cluster of shots, taken at 9:20AM on May 29. Figure 5a contains the vertical component response, and b-c contain the two horizontal components. Plotted are the mean trace in the time domain, bounded by dashed lines which represent $3 \times$ the standard deviation of the repeated shots (in this case 5). Figure 6, which contains the amplitude spectra of the responses, is set up likewise.

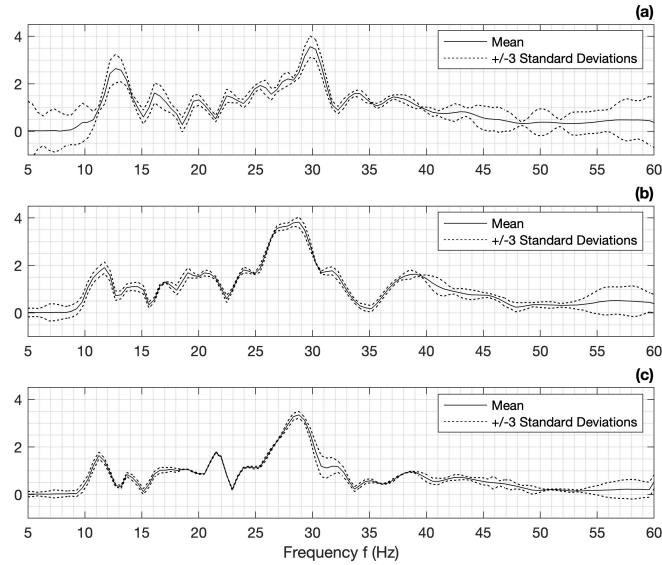


FIG. 6. Mean (solid) plus and minus three standard deviations (dashed) spectra from the 9:20AM 6-shot monitoring survey, geophone level 6 of 24. (a) Vertical component; (b) first horizontal component; (c) second horizontal component.

These results are, of all the monitoring shot clusters, the least repeatable, i.e., the ones with the largest spread between the 6 standard deviations (minus 3 to plus 3). We interpret this to have been caused by changes to the till at and around the Vibe pad, as it is gradually packed down by the sweep. Because of the relatively large data variance, in later analysis we will have to pay slightly closer attention to the 9:20AM cluster, ensuring that any observed variability we wish to interpret lies well outside of this scatter.

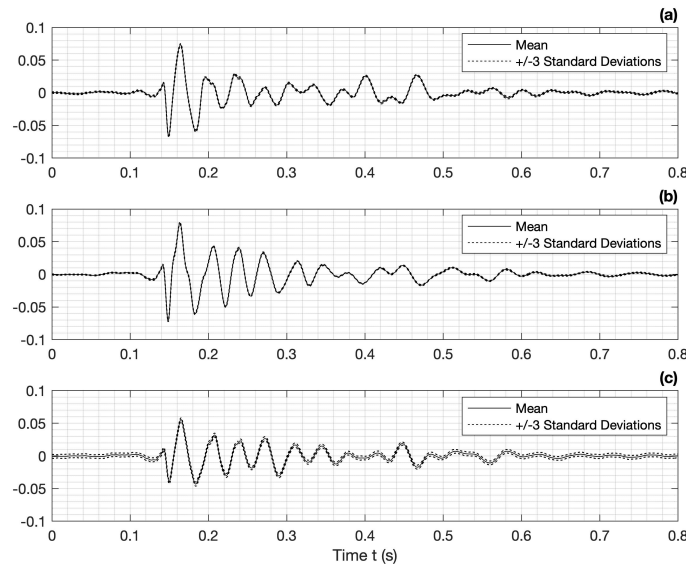


FIG. 7. Mean (solid) plus and minus three standard deviations (dashed) traces from the 1:30PM 6-shot monitoring survey, geophone level 6 of 24. (a) Vertical component; (b) first horizontal component; (c) second horizontal component.

The repeatability improved significantly for all monitoring clusters after the first. Fig-

ures 7-8, which are set up in the same way as the previous two figures, are the mean and $\pm 3 \times$ standard deviations of the 1:30PM May 29 cluster. These are representative of the general repeatability after 9:20AM. The differences between the repeated shots are very small; 6 standard deviations are essentially invisible to the eye at the scales in the Figures. The means and standard deviations determined here will in the next section form the data points and error bars we use when identifying meaningful time-lapse changes.

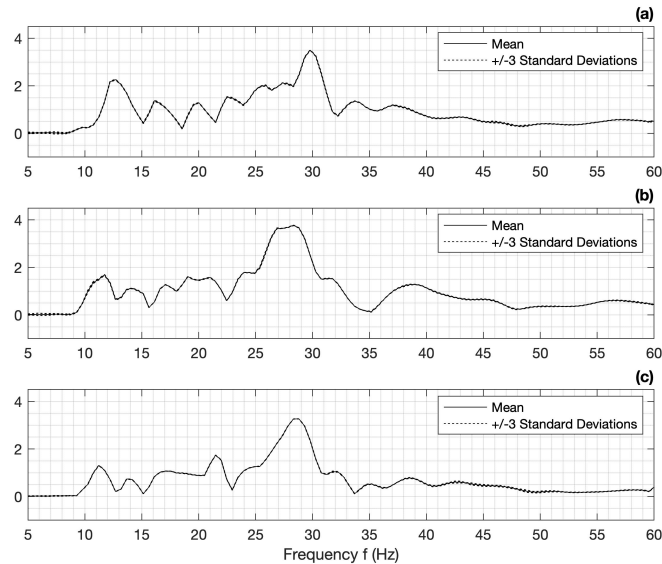


FIG. 8. Mean (solid) plus and minus three standard deviations (dashed) spectra from the 1:30PM 6-shot monitoring survey, geophone level 6 of 24. (a) Vertical component; (b) first horizontal component; (c) second horizontal component.

SIGNIFICANT TRANSIENTS AND TIME LAPSE CHANGES

We observe several transient and time-lapse changes on this backdrop of (1) accurate repeatability and (2) controlled injection timeline, i.e., over the course of the 160hr experiment. We divide these phenomena up into transient and non-transient groups, with the latter corresponding to changes which appear and then remain, and with the former corresponding to changes which track more or less with the pressure, and vanish as it relaxes. Of course, by “non-transient” we really mean something weaker – “non-transient on a 160hr time scale”. In this section we remain entirely empirical, and show some examples of these changes without engaging in any theorizing about their origins. In the next section we will correlate the transients with the pressure data.

Spectral transient: geophone level 17, vertical component, 27Hz

Based on our expectations regarding the size and extent of the pressure and fluid plumes immediately after injection commences, we focus on the lower of the available geophones as being more likely to be sensitive to variations imparted to the wave field. In fact if a candidate variation is weaker up shallow, and stronger deeper, we will view this as circumstantial evidence that the change is associated with the plumes.

The first and main observation is that transients do occur; these variations are visible

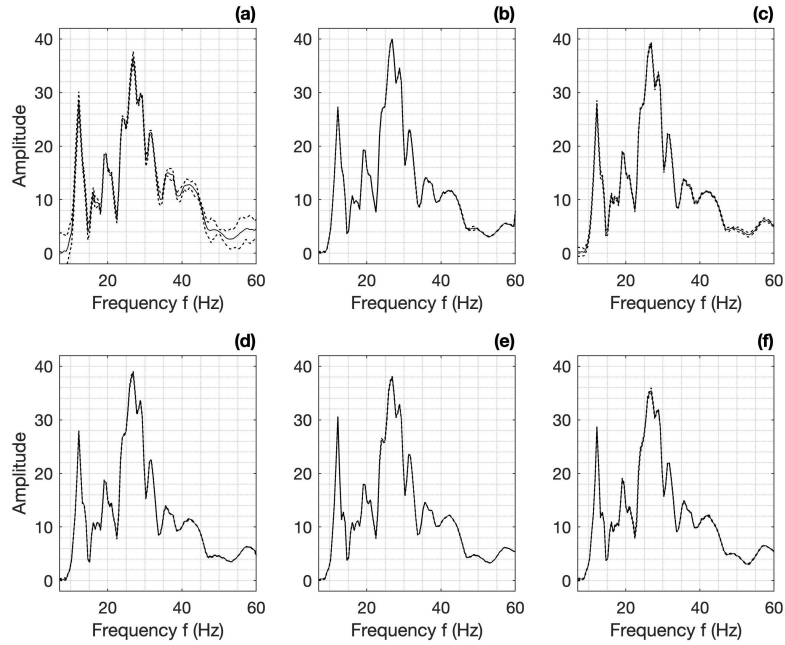


FIG. 9. Spectra from the vertical component of the geophone at level 17 (roughly 275m depth), at monitoring shot numbers (a) 1; (b) 5; (c) 8; (d) 9; (e) 11; and (f) 14. See Table 1 for times/dates.

when the traces (i.e., the time-domain geophone signals) are inspected, but we will focus on the spectral variations, as it is in the frequency domain that the regularities in the transients are most clearly visible. The goal is to hold as many aspects of the experiment as possible fixed, and analyze the data for changes which we can tie to injection. Therefore, in any given example, we will select a geophone level and component, and examine the spectra as functions of the time of the monitoring shot clusters (see Table 1, and/or the horizontal locations of the blue circles in Figure 2). In Figures 9a-f, the spectra (mean and \pm standard deviation curves) of the vertical component of the 3C geophone at level 17 for a representative 6 of the 14 shot clusters are plotted. By eye the spectra appear relatively stable, but there are certain frequency bands in which transient changes are notable.

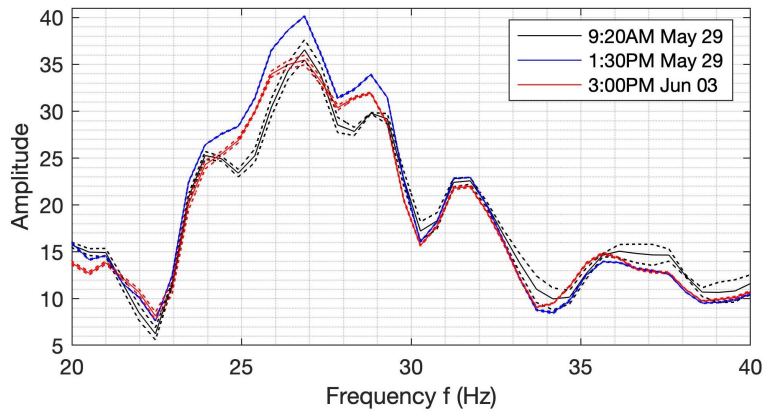


FIG. 10. Three spectra, selected from Figure 9 and overlain. Black: monitoring shot cluster 1 (first); red: cluster 14 (last); blue: midway through experiment, near maximum pressure.

We focus on the 20-40Hz range, in particular the peak frequency at 27Hz. Here we

observe a smooth transient change which appears at the onset of the pressure/injection, and lapses back to approximately its original state by the end of the experiment. In Figure 10, the first, middle, and last spectra are plotted; the black and red curves are the first and last respectively. They are not identical, but in most regions, including at the peak frequency, they fall within each others' standard deviations. The middle (blue) shot also matches the red and black curves in most regions of the spectrum, but in the vicinity of the peak frequency there is a significant increase in amplitude. Let us focus on the peak frequency, which is at 26.9Hz.

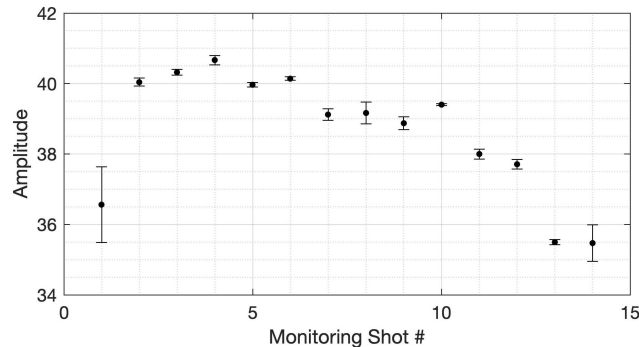


FIG. 11. Mean amplitudes at peak frequency (26.9Hz) with error bars, for each monitoring shot cluster (vertical component, level 17).

Going through each of the 14 monitoring shot clusters, extracting the amplitude spectrum value at the peak frequency (and its error bars based on the standard deviation), and plotting them as a function of monitoring number, we derive Figure 11. The trend to anomalous growth followed by gradual relaxation is evident. The importance of the first monitoring shot cluster to the establishment of the trend is evident here also. We note that the scatter at that point, though relatively large, does not affect the identification of the trend.

Depth dependence

The trend is much less clear at more shallower geophone levels. For instance, at level 8 (roughly depth 230m), the effect is diminished, and when error bars, as before based on variance within shot clusters, is added, the trend is almost completely lost. In Figure 12, the amplitudes at peak frequency (which is closer to 30Hz up shallow) are almost unchanging.

This is clearer in the plot of amplitude at peak frequency versus monitoring shot number in Figure 13. Although a growth and decay still appears as a feature larger than the variance for the monitoring points 2 - 14, it is less clear. Monitoring shot 1 adds quite a lot to the establishment of a growth-relaxation trend, but the error bars are too large to attach too much significance.

Spectral transient: geophone level 17, horizontal component, 25Hz

Returning to the deeper geophone levels, of which level 17 is optimal (meaning, the deepest geophone producing the highest fidelity data with the best reproducibility within

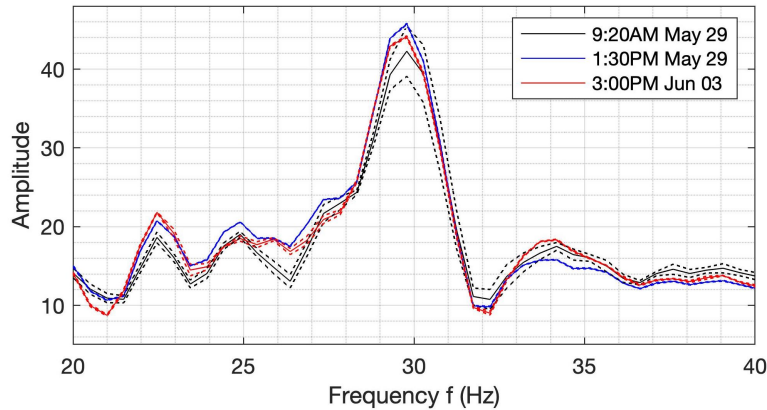


FIG. 12. Three spectra, similar to those in Figure 10, but from a shallower geophone (level 8), are overlain. Black: monitoring shot cluster 1 (first); red: cluster 14 (last); blue: midway through experiment, near maximum pressure.

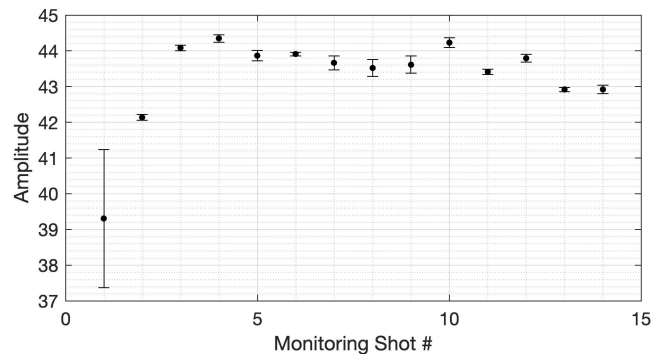


FIG. 13. Mean amplitudes at peak frequency (29Hz) with error bars, for each monitoring shot cluster (vertical component, level 8).

monitoring shot cluster), we can see similar features in the horizontal component at a slightly lower frequency. The H2 component of the level 17 geophone has the mean \pm standard deviation spectra, between 20-40Hz, plotted in Figure 14. Here, again, the black and the red curves correspond to the spectra at the beginning (0hr) and end (160hr) of the injection experiment. The blue curve is the spectrum at near the time at which the injection pressure is at a maximum.

The 25Hz spectral peak is focused on. The mean amplitude and the standard deviations are plotted for each of the monitoring shot points in Figure 15. At level 17 a similar trend to that in the vertical component is visible. Fortunately at these geophones the variance within monitoring shots is relatively low also, so the trend seems more certain.

Inspection of the spectra in Figure 14 reveals more complexity in the response than simply the peak frequency behaviour. In the lower frequency ranges a range of variability is also visible. These remain under examination. Some of the changes we see appear to fall into the category of non-transients – for instance the transition from black to blue to red between 10-15Hz does not “relax” by the 160hr end point of the experiment, in the sense of returning to its baseline (black curve) state. The question of whether these are in

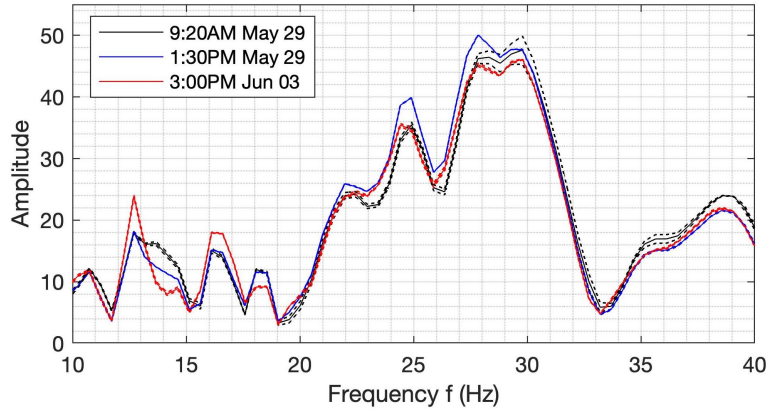


FIG. 14. Three spectra, similar to those in Figure 10, but from the second horizontal component. Black: monitoring shot cluster 1 (first); red: cluster 14 (last); blue: midway through experiment, near maximum pressure.

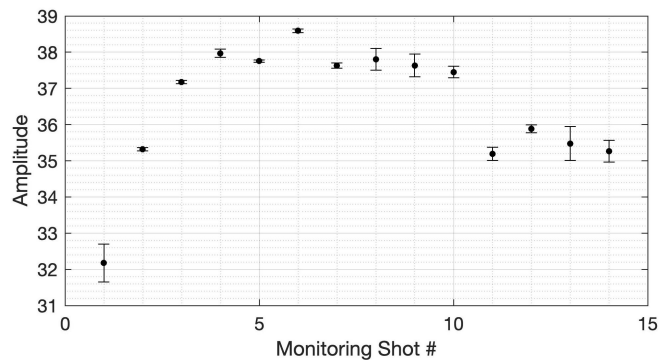


FIG. 15. Mean amplitudes at peak frequency (25Hz) with error bars, for each monitoring shot cluster (horizontal component, level 17).

some sense permanent, or whether they are transient but the relaxation time is longer than 160hrs, is not constrained by our current experiment.

CORRELATION WITH INJECTION PRESSURE

The question we are interested in pursuing with this experiment has been: given that we have direct measurements of the injection pressure at the injection point, and that we appear to have amplitude spectral variations associated with the pressurization of the well, are there meaningful correlations between the two?

To answer this question we examine the pressure data alongside the peak amplitudes in both the vertical and horizontal components. These are plotted in Figures 16-17 respectively. The amplitudes indeed track pressure changes convincingly.

TOWARDS INTERPRETATION

In the 2018 microbubble water report, clear evidence of a boost of high frequencies and a degradation of low frequencies was noted; this was the particular pair of features

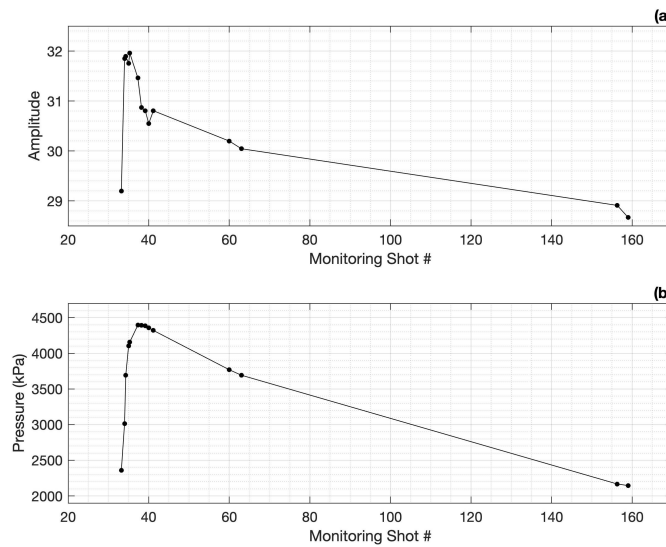


FIG. 16. Correlation of (a) peak spectral amplitude (vertical component, level 17) and (b) injection pressure as a function of hours since 12:00AM May 28.

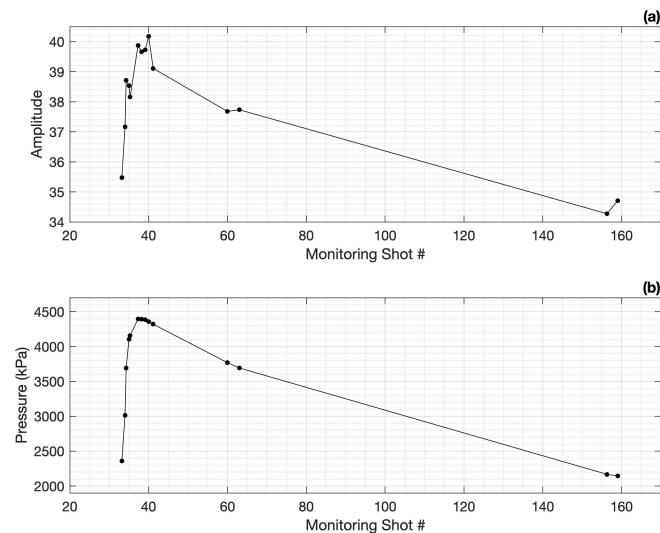


FIG. 17. Correlation of (a) peak spectral amplitude (horizontal component, level 17) and (b) injection pressure as a function of hours since 12:00AM May 28.

of the waveform change which were difficult to explain, and for which we introduced the possibility of elastic bracing. In the more careful CO_2 experiment we clearly see some relative changes in the spectra which appear to be connected to the injection—but do they have any of these strange characteristics which led us to attempt modelling with a Klein-Gordon type equation?

In fact, there are. Just as in the November 2018 CaMI experiment, there is evidence of a simultaneous drop in low frequency amplitude and growth in high frequency amplitude. (Also like the November 2018 case, the phenomenon is more subtle than in the microbubble water experiment.) To see it, let us return to the second horizontal component and its amplitude variation as measured at the deepest level at which the data were good (level 17). In Figure 18, the amplitude spectral values at 14Hz (black) and 25Hz (blue) are compared,

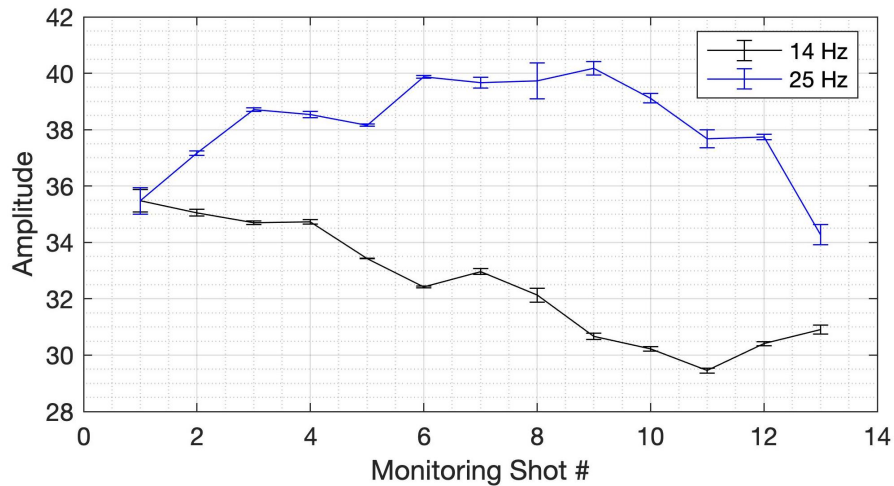


FIG. 18. Amplitude spectral values at low frequency (14Hz) in black, versus, high frequency (25Hz) in blue. The low frequency amplitude has been shifted upward so that the amplitudes have the same value at monitoring shot point 1, so that the relative amplitudes can be observed on a single plot.

with their standard deviations again included as error bars. In this case the amplitude at 14Hz has been adjusted with an additive constant such that it agrees with the 25Hz curve at monitoring shot number 1. This allows the two amplitudes’ relative values to be easily observed on the same plot. We thus confirm a drop in low frequency amplitude simultaneous to a growth in high frequency amplitude, both of which relax as the end of the 160hr experiment approaches.

CONCLUSIONS

Last year we reported on an unusual time-lapse data set, in which waveforms transiting microbubble injection underwent several difficult-to-explain alterations. In addition to attempting to explain these phenomena, we also undertook to seek similar variations in seismic waveforms propagated through the plumes of CO₂ being injected into the 300m formation at the CaMI-FRS in Newell County AB. We established remarkable repeatability with the Envirovib source placed pad-down throughout the 160hr experiment.

We identify several spectral variations, some of which appear and then vanish over the course of the experiment; of these many exceeded several standard deviations as estimated during repeatability tests, and are labelled “real” variations connected to the injection. The changes are in general consistent with our 2018 “elastic bracing” explanation, but they appear to be much more complicated and quite subtle, and it is less clear that a Klein-Gordon bracing mechanism should be introduced. Perhaps the best way to put it is, if presented with this data in isolation it is unlikely the bracing mechanism would have occurred to us.

Nevertheless, in particular instances we observe a striking tendency for the low frequency amplitudes at geophones near the injection to drop, while the high frequencies grow, well outside of the variance associated with repeatability; furthermore, this effect grows and then decays tracking the injection pressure. We feel confident asserting that the

presence of the pressure and fluid plumes are, like the microbubble water, causing significant and unusual changes to the seismic waveform interacting with it.

ACKNOWLEDGEMENTS

We thank the sponsors of CREWES for continued support. This work was funded by CREWES industrial sponsors, NSERC (Natural Science and Engineering Research Council of Canada) through the grant CRDPJ 461179-13, and in part thanks to the Canada First Research Excellence Fund. The data were acquired at the Containment and Monitoring Institute Field Research Station in Newell County AB, which is part of Carbon Management Canada.

REFERENCES

- Byerley, G., Monk, D., Aaron, P., and Yates, M., 2018, Time-lapse seismic monitoring of individual hydraulic frac stages using a downhole DAS survey: *The Leading Edge*, **37**, No. 11, 802–810.
- Innanen, K. A., Nakata, R., Kato, A., Lawton, D. C., and Bertram, M., 2019, Seismic evidence for transient elastic bracing in microbubble water and CO₂ injection zones: *SEG Expanded Abstracts*.
- Landrø, M., 2001, Discrimination between pressure and fluid saturation changes from time-lapse seismic data: *Geophysics*, **66**, No. 3, 836–844.
- Lumley, D., 2001, Time-lapse seismic reservoir monitoring: *Geophysics*, **66**, No. 1, 50–53.
- Morse, P. M., and Feshbach, H., 1953, *Methods of theoretical physics*: McGraw-Hill Book Co.